# Finite Element Analysis of steady state behaviour of squirrel cage induction motors: a comparison with measurements.

R. De Weerdt, E. Tuinman,
Holec Machines & Apparaten,
P.O. Box 4050, 2980 GB Ridderkerk,
the Netherlands

K. Hameyer, R. Belmans,
Katholieke Universiteit Leuven,
Dept. EE, ESAT/ELEN,
Kard. Mercierlaan 94, 3001 Leuven, Belgium

**Abstract**

**The paper describes the steady state analysis of squirrel cage induction motors using a two-dimensional finite element solution. Saturation is included using an iterative process combining both, static and time-harmonic solutions. The motor end-effects are included during the time-harmonic solution as lumped parameters. The influence of the different end-effect parameters is analysed by including or neglecting them in the calculations. Both motors, with closed and open rotor slots are analysed. Different operating points for load, no-load and locked rotor situations are analysed and compared. Good agreement with measurements is found. A commercial FEA package is used.**

## Introduction

In the last decade, the analysis of squirrel cage induction motors using finite elements has received much attention. The finite element method is used to calculate the electromagnetic fields in parts of the motor or of the full motor. The calculations of parts of the motor often have the purpose to verify or correct existing analytical or empirical formulae Examples are the calculation of the Carter factor for various slot shapes [1] or the calculation of the rotor bar impedance taking saturation and skin-effect into account [2]. The analysis of the steady state behaviour is most often based on the electromagnetic field calculation of a cross-section of a part of the motor (mostly one pole pitch). A three dimensional calculation is not considered because the model size would lead to unacceptable computational costs. An accurate and realistic solution requires the following effects:

1) Induced rotor currents
2) Saturation
3) Motor end-effects

To combine both, saturation and induced currents, theoretically, a transient solution is required. This however results in high computational costs. Therefore, several approximated methods are developed [3,4]. The iterative method described here is a combination of static (non-linear) and time-harmonic (linear) solutions [5]. A third aspect to be included in the analysis are the motor end-effects (stator end-winding impedance and end-ring impedance). Values for these end-effect parameters are most often obtained from empirical formulae, but can also be calculated by two- and three dimensional field analysis [6,7]. This latter option is applied here and results in a more accurate description of the end-effects. The variation of the ring resistance due to the skin-effect or the variation of the end-winding leakage for different load conditions are otherwise difficult to asses. Using the finite element method for both, the end-effect and the field in the cross-section of the motor results in an analysis purely based on simulations. When this analysis is found to be in good agreement with reality, it can be used instead of prototyping. This results in a substantial cost reduction. To verify this, a detailed comparison with measurements is required. The influence of the different end-effect parameters is shown by including or neglecting them in the analysis. The same is done with saturation.

## Finite Element Analysis

Four-pole traction motors having 48 stator slots and 40 rotor slots are modelled. The rotor winding consists of solid copper bars without skewing. Both motors, with closed and open rotor slots are analysed. A two dimensional model describing the cross-section of the motor is used. Applying the appropriate boundary conditions, only one pole pitch has to be modelled. Figure 1 shows the outline of one of the models used, together with the boundary conditions.

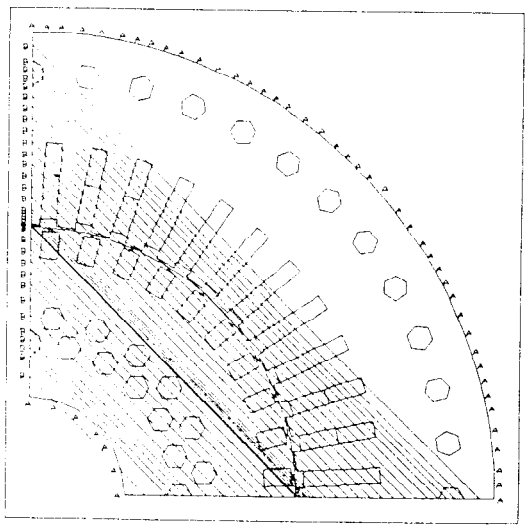

Fig. 1: Outline and constraints of a one pole pitch finite element model of a squirrel cage induction motor.

### Combination of saturation and induced currents

To combine both, the influence of induced currents and saturation, an iterative process using both, time-harmonic and static solutions is used [5]. The time-harmonic solver yields the induced rotor currents. From the solution the real and imaginary component of both, stator and rotor currents are extracted and used as excitation for two static non-linear problems. By averaging, the reluctivity in

each element is determined. The reluctivity vector obtained is used as a temporary operating point for a next time-harmonic (linear) solution. The described procedure is found to converge in less than five steps and is more robust than the method of successive underrelaxation [8]. It is used for both, current driven and voltage driven problem formulations, for all load conditions. The procedure can either start with the static calculations (in that case initially no rotor currents are assumed) or with the time-harmonic calculation. The latter is advantageous when the rotor has open rotor slots. When the rotor has closed slots a linear calculation provides rotor currents that are much smaller than rated and will not influence the next static solution. Therefore, when closed slots are applied, the iteration process should start with the static problems. Figure 2 shows the flow-chart of the procedure when starting with the time-harmonic problem definition.

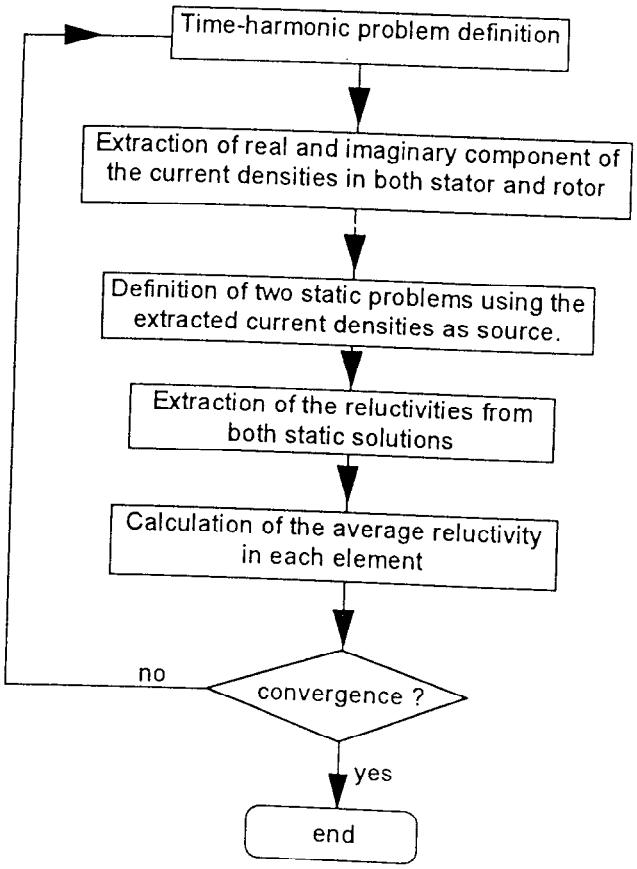


Fig. 2: Flow-chart of the iterative process to combine both, induced currents and saturation using static and time-harmonic solutions.

The described procedure is shown to give similar results as the more conventional method of effective reluctivities [3].

## Influence of the end-effects

The time-harmonic solution procedure consists of the finite element problem combined with a set of circuit equations describing the motor end-effects. The end-effects included in the calculations are resistance and leakage inductance of both end-winding and end-ring. The end-effects are included as lumped parameters. Values for the parameters are obtained by 2D and 3D finite elements computation [7] The influence of each separate end-effect parameter is examined by including or neglecting it. The finite element analysis is performed for both closed and open slots.

## Calculation of the end-effect parameters

The calculation of the end-effect parameters is performed using 2D and 3D finite elements except for the end-winding resistance, that is calculated analytically. The end-winding leakage and the end-ring leakage are calculated using a 3D model describing one pole pitch of one end-winding region. Both leakage components are calculated for different load conditions. An important variation in both parameters is noticed due to the load-dependent coupling between stator end-winding and rotor end-ring [7,9]. This coupling between end-winding and end-ring should theoretically be incorporated in the magnetising inductance, but is negligible since the coupling mainly takes place in air. By far the most important end-effect parameter in a squirrel cage induction motor is the end-ring resistance. This parameter is calculated using an analytical approximation, a 2D (axisymmetric) and a 3D finite element calculation , also for different load conditions. Significant differences are obtained [3] when skin effect becomes important (starting conditions). Figure 3 shows the increase in resistance for the three calculation methods.

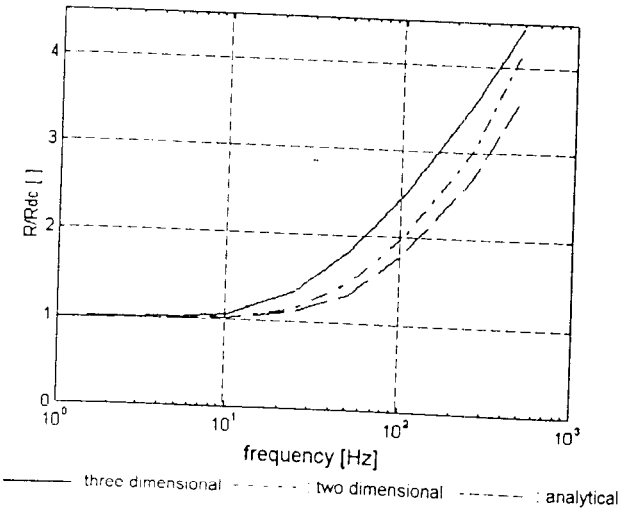


Fig. 3: Variation of the ring resistance with respect to the dc-value as a function of the applied frequency.

As the 3D approach is the only one having the current input correctly modelled (via the bars), it is considered the most accurate.

## No-load analysis

For the no-load analysis, the conductivity in the rotor winding is set to zero. The end-effects taken into consideration are the stator end-winding inductance and resistance. The full end-winding inductance acts as leakage in this situation. Figure 4 shows the calculated and measured no-load characteristic. The motor has closed rotor slots. It can be seen that the non-linear behaviour of the motor at no-load is correctly modelled. The end-winding parameters have little influence on the overall result (less than 5 %) because the end-winding leakage is only a few percent of the magnetising inductance.

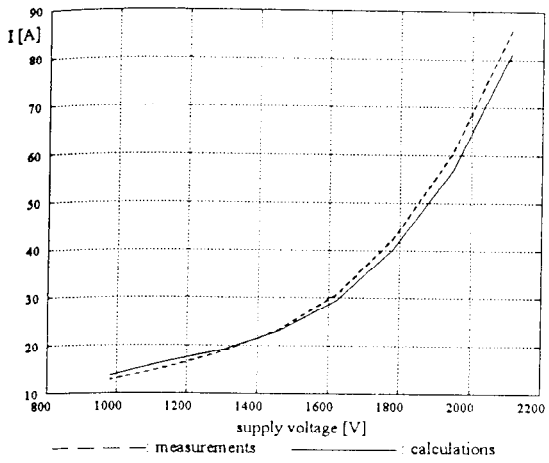


Fig. 4: Calculated and measured no-load characteristic.

## Load calculations

For the load calculations, different operating points, at various slip s are compared with measurements. To obtain the induced currents in the rotor bars, a time-harmonic solution is used as described above. Such a solution requires that only one frequency is specified. During load operation however, the frequency of the stator currents equals the supply frequency, while the rotor current frequency is the slip frequency. Two approaches are possible to resolve this problem. Consider first the equation solved by the 2D time-harmonic solver.

$$\nabla\cdot(\nu\nabla A_z) - j\omega\sigma A_z = -J_{s,z} \qquad (1)$$

Here $A_z$ is z-component of the vector potential A, $\sigma$ is the conductivity, $\omega$ is the pulsation $J_{s,z}$ is the source current and $\nu$ is the reluctivity. To obtain the correct induced currents, the slip pulsation $s\omega_n$ ($\omega_n$ is the supply pulsation) could be applied in (1).

$$\nabla\cdot(\nu\nabla A_z) - js\omega_n\sigma A_z = -J_{s,z} \qquad (2)$$

For a voltage driven problem formulation, the application of the slip pulsation is not sufficient. When the slip pulsation is used, the flux variation on the stator will also take place with this pulsation resulting in a back-EMF that is 1/s times smaller than required. Therefore, the applied voltage $U_n$ has to be scaled down to $sU_n$. In order to maintain the correct ratio between back-EMF and resistive voltage drop, the resistivity of the stator winding has to be scaled down in the same way. The same rotor and stator currents are obtained by applying the supply frequency and at the same time using $s\sigma$ as the conductivity in the rotor [3]. This approach is used here since it only requires the modification of the rotor conductivity, whereas the supply voltage and stator resistance keep their rated value. It should be noted that the modified conductivity should also be used to calculate the rotor end-ring resistance and the resistance of the bar ends outside the rotor core. Because the conductivity used during solving is 1/s times smaller than in reality, the Joule-losses obtained are 1/s times larger. Current redistribution in the rotor bars is modelled correctly in both cases since the skin depth is a function of the product of pulsation and conductivity.

## Comparison with measurements

Figure 5 shows the calculated and measured torque for a motor with open rotor slots.

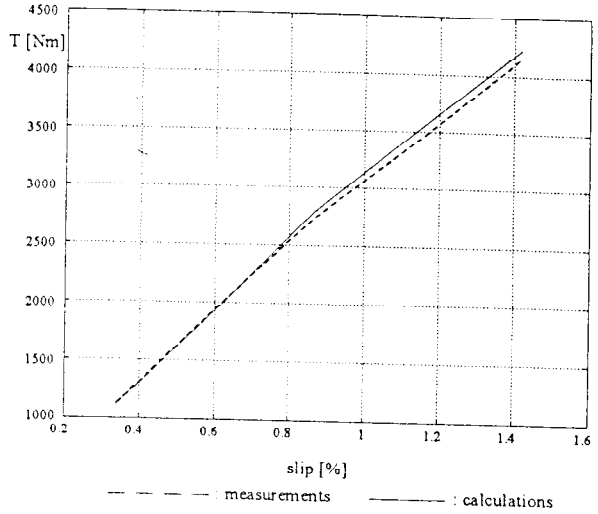


Fig. 5: Calculated and measured torque for a 400 kW traction motor.

The generated torque is calculated from the Joule-losses in the rotor instead of using the Maxwell stress tensor in the airgap because a first order solution is used resulting in a zero order solution of the magnetic flux density B.

## Influence of saturation

The importance of the inclusion of saturation in the calculations is shown by comparing the field plot of the linear solution with the non-linear calculation. Figures 6 and 7 show the field plot at rated load of a 146 kW traction motor having closed rotor slots.

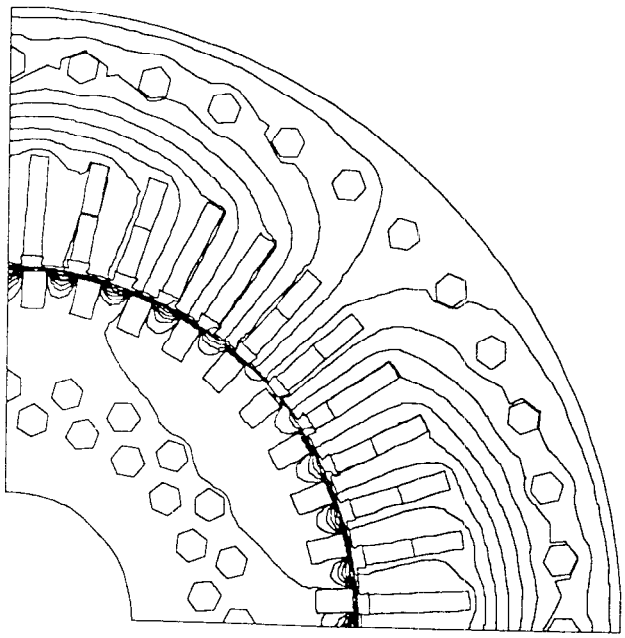

Fig. 6: Field plot at rated conditions of a motor with closed rotor slots (linear calculation).

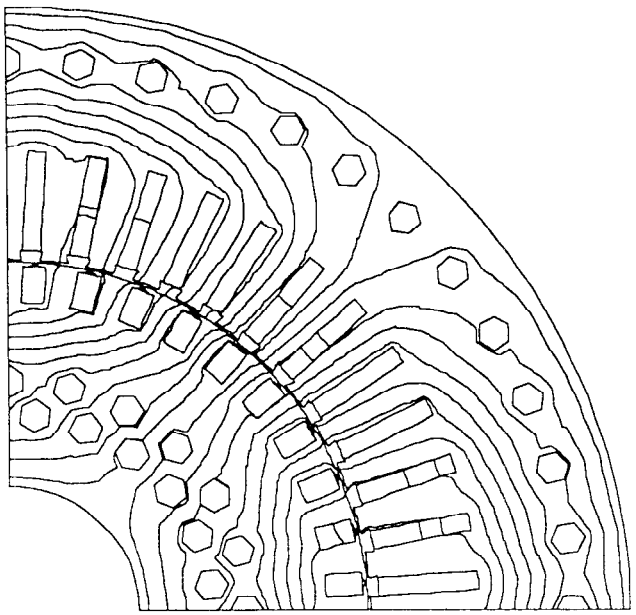

Fig. 7: Field obtained at rated load (non-linear calculation).

**Influence of the end-effect parameters**

For the load calculations, both stator and rotor end-effects have to be examined. The most important end-effect parameter is the end-ring resistance. Calculations show that more than 30 % of the Joule losses in the rotor are located in the bar ends outside the rotor core and in the end-ring. Knowing that the generated torque of the motor is proportional to the rotor Joule losses, it is clear that an accurate calculation of the end-ring resistance and a correct inclusion of its effects is essential. Furthermore, it can be stated that the end-ring leakage is of no importance during load operations, due to the small slip frequency. The influence of the end-winding impedance remains small as in the no-load calculations. This is enforced by the fact that the end-winding leakage is smaller during load operations.

## Locked rotor calculations

For motors having open rotor slots, the locked rotor behaviour is approximately linear. Therefore, the above described procedure converges in two iteration steps. For motors with closed rotor slots, the saturation cannot be neglected, the behaviour is non-linear. Also the influence of the different end-effect parameters is different for both types of motors.

**Comparison with measurements**

Figure 8 shows the calculated and measured inductance at the stator terminals for a motor with closed slots. Also in this case, the non-linear behaviour is appropriately modelled. For most operating points, good agreement with measurements is found. The non-linear behaviour of the motors with closed rotor slots is mainly due to an additional leakage component, the bridge leakage. This leakage component is strongly load dependent [2].

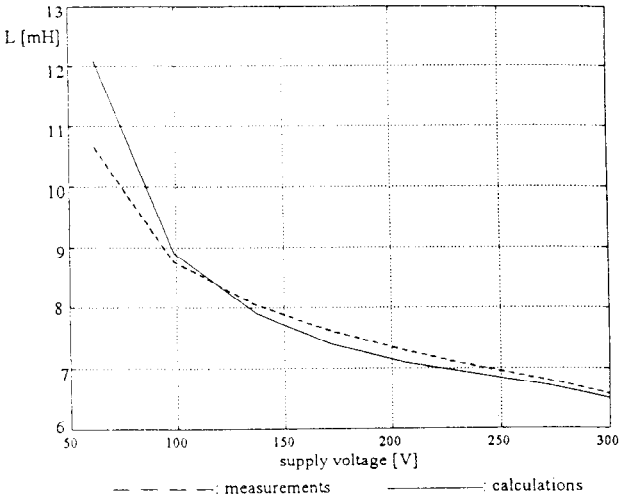


Fig. 8: Calculated and measured inductance at locked rotor operation (motor with closed rotor slots).

**Influence of the end-effect parameters**

During locked rotor operation, none of the end-effect parameters can be neglected even though the leakage components of end-winding and end-ring are at their smallest value. The coupling between rotor end-ring and stator end-winding obtains its highest value at locked rotor operation. Therefore, the leakage parts of end-winding inductance and end-ring inductance are at their minimum value [7,9]. Table 1 shows the end-effect parameters used at locked rotor operation.

Table 1: End-effect parameters at locked rotor operation.

| end-ring resistance | end-ring leakage | end-winding resistance | end-winding leakage |
|---|---|---|---|
| 20 μΩ | 0.3μH | 43 mΩ | 0.4 mH |

Table 2 shows a comparison of calculated and measured values for the stator current I, the supply power P, inductance L and resistance R at locked rotor operation. The influence of the different end-effect parameters is shown by including them one by one in the calculations. Table 2 refers to a motor with open rotor slots.

Table 2: Comparison between calculated and measured locked rotor operation. (a) calculations, (b) measurement

| | I[A] | P [kW] | L [mH] | R [mΩ] |
|---|---|---|---|---|
| (a1) | 197.4 | 16.1 | 2.6 | 138 |
| (a2) | 160.4 | 10.8 | 3.0 | 140 |
| (a3) | 159.4 | 14.0 | 3.1 | 184 |
| (a4) | 158.7 | 15.6 | 3.1 | 207 |
| (a5) | 152.9 | 14.2 | 3.2 | 207 |
| (b) | 152.0 | 14.3 | 3.2 | 208 |

The different calculations of table 2 are:
(a1) no end-effects
(a2) end-winding resistance
(a3) end-winding impedance
(a4) (a3) plus inclusion of end-ring resistance
(a5) all end-effect parameters

The influence of the end-effect parameters is clear, only when all parameters are considered, a good agreement with measurements is found. Unlike in the load or no-load calculation, the end-ring leakage has a distinct influence at locked rotor operation. This is only found for motors

with open slots. Due to the bridge leakage the influence of the end-ring leakage is much smaller for motors with closed rotor slots.

## Conclusions

The analysis of several squirrel cage induction motors is performed and compared with measurements. The end-effect parameters are calculated using 3D finite element analysis and then are included as lumped parameters in the 2D analysis. The influence of the different end-effect parameters is examined at different operating conditions. The effective end-ring resistance can double at locked rotor operation when compared with the dc-resistance, used during load operation. Furthermore only the leakage components of the end-winding inductance and end-ring inductance have to be considered. Both strongly depend on the load condition. By including or neglecting the end-effect parameters in the 2D analysis, the following rules are found:

The influence of the end-winding impedance at no-load is noticeable but rather small (less than 5%).

At load, the most important parameter is the end-ring resistance. The end-winding inductance has little influence. The end-ring inductance can be neglected.

At locked rotor, all end-effect parameters have a significant influence on the motor behaviour. A distinction must be made between open and closed rotor slots regarding the influence of the end-ring inductance. For most of the operating points, the end-ring inductance can be neglected if the rotor has closed slots. This is due to the fact that these motor have an additional leakage component, the bridge leakage, but this component is strongly load dependent [5]. Good agreement between measurements and simulations is found, for both motors with open and closed rotor slots, under all operating conditions.

## Acknowledgment

The authors are indebted to the Belgian "Nationaal Fonds voor Wetenschappelijk Onderzoek" for its financial support for this work, to the Belgian Ministry of Scientific Research for granting the project IUAP No. 51 on "Magnetic Fields" and to Holec Machines & Apparaten, Ridderkerk, the Netherlands.

## References

[1] S.C. Tandon, E. Richter, M.V.K. Chari: "Finite elements and electric machine design", *IEEE Trans. on Magnetics*, Vol. 16, No. 5, 1980, pp. 1020-1023.

[2] S. Williamson and M.C. Begg, "Calculation of the bar resistance and leakage reactance of cage rotors with closed slots," *IEE Proc.* Vol. 132, Pt. B, No. 3, 1985, pp. 125-132.

[3] E. Vassent, G. Meunier, J.C. Sabonnadière, "Simulation of induction machine operation using complex magnetodynamic finite elements," *IEEE Trans. on Magnetics*, Vol. 25, No. 4, 1989, pp. 3064-3066.

[4] J. Luomi, A. Niemenmaa, A. Arkkio: "On the use of effective reluctivities in magnetic field analysis of induction motors fed from a sinusoidal voltage source", *Proc. ICEM München,* 1986, pp. 706-709.

[5] R. Belmans, R. De Weerdt and E. Tuinman, "Combined field analysis techniques and macroscopic parameter simulation for describing the behaviour of medium-sized squirrel-cage induction motors fed with an arbitrary voltage," EPE Brighton, September 1993, pp. 413-418.

[6] S. Williamson and M.A. Mueller, "Calculation of the impedance of rotor cage end-rings," *IEE Proc.* Vol. 140, Pt. B, No. 1, 1993, pp. 51-60.

[7] R. De Weerdt and R. Belmans, "Squirrel cage induction motor end-effects using 2D and 3D finite elements," EMD Durham, September 1995.

[8] R. De Weerdt, K. Brandiski, U. Pahner and R. Belmans, "Comparative analysis of two methods for time-harmonic solution of the steady state in induction motors," *J. Appl. Phys.* 75 (10), Proc. of the 38th Annual Conference on Magnetism and Magnetic Materials, p. 6050.

[9] S. Williamson, M.A. Mueller: "Induction motor end-winding leakage reactance calculation using the Biot-Savart method, taking rotor currents into account", *Proc. ICEM conf. 1990,* Vol. 1, pp. 480-484.